

Dark-Field Imaging on a Clinical CT System: Performance and Potential based on first Results

Nikolai Gustschin^{a,b}, Manuel Viermetz^{a,b}, Clemens Schmid^{a,b}, Jakob Haeusele^{a,b},
Frank Bergner^d, Tobias Lasser^{b,c}, Thomas Koehler^{d,e}, and Franz Pfeiffer^{a,b,e,f}

^aChair of Biomedical Physics, Department of Physics, Technical University of Munich, 85748 Garching, Germany.

^bMunich Institute of Biomedical Engineering, Technical University of Munich, 85748 Garching, Germany.

^cComputational Imaging and Inverse Problems, Department of Informatics, Technical University of Munich, 85748 Garching, Germany.

^dPhilips Research, 22335 Hamburg, Germany.

^eInstitute for Advanced Study, Technical University of Munich, 85748 Garching, Germany.

^fDepartment of Diagnostic and Interventional Radiology, School of Medicine and Klinikum rechts der Isar, Technical University of Munich, 81675 München, Germany.

ABSTRACT

X-ray computed tomography (CT) has been established as a daily tool in clinical diagnostics and has been continuously refined by more recent innovations in the last years. These systems are, however, limited by fundamental constraints since they are only capable of mapping X-ray attenuation differences in the tissue. Phase-contrast and dark-field imaging provide complementary contrast, which originates from physically different interaction processes of X-rays with matter. Particularly the dark-field signal is considered to have significant diagnostic potential since it is capable to retrieve micro-structural information below the actual resolution limit of the imaging system. This was demonstrated in various laboratory setups and recently also in the first study with human patients in a clinical radiography system based on a grating interferometer. In a recent work, we presented the first implementation of such an X-ray interferometer into a clinical CT gantry. Upscaling and adapting this technology for a rotating CT gantry involves several challenges and tradeoffs ranging from limitations in interferometer design over fast, continuous signal acquisition requirements to tolerances in applied patient dose. In this work we discuss the performance of the first clinical dark-field CT prototype. For this purpose, we present results of our phantom studies which were designed to evaluate whether and how the dark-field contrast generated by the system is capable to provide additional structural sample information. The key aspects include the possibility of quantitative imaging and a gradual approach to simulate results that come as close as possible to a real application in a human patient.

Keywords: X-ray imaging, dark-field contrast, computed tomography

1. INTRODUCTION

X-ray computed tomography has evolved to one of the most commonly used and indispensable diagnostic 3D imaging modalities. Moreover, the technique is continuously optimized by recent innovations like dual energy or photon-counting technologies as well as advanced data acquisition, reconstruction, and evaluation procedures. Those are, however, still based on a contrast which is measured by retrieving the X-ray attenuation properties of different tissues and hence fundamentally limited. Considering the wave nature of X-rays, additional and complementary contrast can be achieved by measuring the small-angle scattering (dark-field) properties of an object.¹ Contrary to attenuation contrast, the dark-field signal hence retrieves information on micro-structures without the need to actually resolve them on the detector.² The potential of the dark-field channel in clinical

Send correspondence to Nikolai Gustschin (niko.gustschin@tum.de)

diagnostics has been discussed in various studies, which were mainly focused on lung diseases like chronic obstructive pulmonary disease (COPD),^{3,4} fibrosis⁵ or lung cancer.⁶ This is because, particularly in lung parenchyma, the dark field signal is significantly more sensitive to small changes in the alveolar structure compared to the attenuation.

One of the most promising approaches for dark-field imaging with respect to clinical applications is Talbot-Lau interferometry.⁷ While first clinical prototypes of this kind are limited to 2D radiographic imaging, all bench top or small-animal CT systems feature a step and shoot data acquisition which leads to total scan times of at least several minutes, which is unfeasible for realistic clinical applications.^{8,9} Recently, we reported on the first successful integration of a Talbot-Lau interferometer into a rotating clinical CT gantry.¹⁰ Restrictions in total interferometer length and grating positioning on a compact CT gantry along with limitations in state of the art grating fabrication technology constrain the theoretically achievable system sensitivity.

Here, we present first results from our prototype system starting from a basic proof-of-concept towards more realistic phantoms for an actual clinical application. This allows to practically evaluate the system performance and discuss its potential and limitations for clinical application. In this context, we also consider a possibility of quantitative dark-field imaging and discuss the patient dose resulting from the applied scanning protocols.

2. DARK-FIELD SIGNAL CALIBRATION

A physical interpretation of the dark-field signal is a scattering distribution, which is continuously broadened along the beam path.¹¹ Similar to the exponential decay of the attenuation signal, the measured dark-field signal therefore depends on the penetrated sample thickness. Compared to 2D radiographic imaging, computed tomography provides a more suitable basis for quantitative imaging. However, the dark-field signal strength further depends on several additional parameters like the feature size of the small-angle scattering structures and also system specific characteristics like the X-ray spectrum or the interferometer sensitivity.² Similar to the attenuation Hounsfield scale, a quantitative consistency between different system parameters can be achieved by a calibration using predefined reference materials.⁸ For this purpose we use a neoprene foam and air as reference materials in order to transform the measured linear diffusion coefficient $\varepsilon(x)$ to a dark-field Hounsfield unit (HUd) according to:

$$\text{HUd}(x) = 1000 \cdot \frac{\varepsilon(x) - \varepsilon_{\text{air}}}{\varepsilon_{\text{neoprene}} - \varepsilon_{\text{air}}}. \quad (1)$$

In this HUd scale, the signal from the strongly scattering and weakly attenuating neoprene is defined by a value of 1000 while the non-scattering air yields a value of zero. Darker regions thereby indicate a lower density of scattering interfaces. For a better differentiation to the attenuation Hounsfield scale (HUa), the HUd scale reference values are chosen such that the signal from lung tissue is expected to give positive values.

3. MULTI-MATERIAL PHANTOM

For a proof-of-principle that the dark-field CT prototype is capable to differentiate a varying density of scattering structures below its resolution limit, we use a multi-material phantom. It is composed of different materials in plastic tubes which are arranged around a larger polyoxymethylene (POM) cylinder. The reconstructed attenuation and dark-field images are shown in Fig. 1a and b and demonstrate that our system is able to retrieve the complementary nature of the dark-field signal. Dry wool for example, has a relatively weak attenuation but strong dark-field signal. A decreasing density is hardly noticeable in the attenuation while it is clearly visible in the dark-field. On the other hand, the dark-field signal also fades with an increasing water content, which gradually neutralizes the amount of scattering interfaces and is more apparent in the attenuation modality.

Similarly, pathological changes in lung parenchyma can either be a loss of pulmonary structures (e.g. emphysema), or a replacement with conjunctive tissue (e.g. pulmonary fibrosis). The example demonstrates that the system can successfully provide perfectly registered multi-modal images which enable a better differentiation of material compositions relevant for diagnostic purposes. Moreover, the results demonstrate that also material inhomogeneities which are hardly noticeable in the attenuation contrast can be more distinctly revealed in the dark-field modality. This is for example apparent in the cylinders stuffed with wool or also in the periphery of the top neoprene cylinder, where the material is locally compressed by a tube housing.

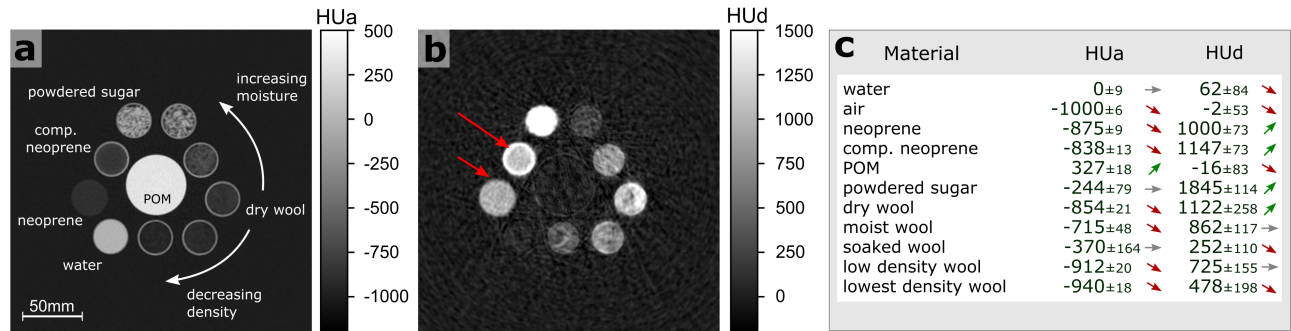


Figure 1. Reconstruction results from a multi-material cylinder phantom. **a**, Conventional attenuation and **b**, dark-field tomograms calibrated to the attenuation Hounsfield (HUa) and dark-field Hounsfield scales (HUd). The dark-field channel maps the scattering power of different materials and hence provides complementary sub-resolution information. The arrows in **b** indicate a locally stronger dark-field signal from the same neoprene material, where it is slightly compressed by the tube housing. **c**, Summary of the measured HUa and HUd units from the reconstruction shown in **a** and **b** including standard deviation. The coloured arrows indicate a rough classification of the signal within the overall measured signal range of the respective contrast modality. They demonstrate that different HUa and HUd signal combinations contain uncorrelated information which can facilitate material differentiation.

4. ANTHROPOMORPHIC THORAX PHANTOM

To evaluate the dark-field CT prototype regarding clinical application, we employed an anthropomorphic human chest phantom. First, it allows us to assess the performance of the system on a large field of view (FOV). Secondly, it also simulates a more realistic attenuation of the incoming photon flux by artificial bones and soft tissue, which is important when it comes to dose and noise considerations. To simulate lung tissue, we modified the commercially available phantom (Lungman, Kyoto Kagaku, Tokyo, Japan)¹² with a neoprene insert. It features a relatively weak attenuation as well as a porous micro-structure in the size range of lung alveoli.¹³ A POM cylinder in the centre simulates additional attenuation by the heart and several plastic tube inserts allow to evaluate additional embedded materials. The respective attenuation and dark-field images are depicted in Fig. 2a and b. The FOV of the prototype system (45 cm) is capable to map the entire human thorax along with the patient table. As expected, the conventional reconstruction yields a good contrast for highly attenuating materials like bones, POM and the artificial soft tissue. In contrast, the scattering properties of the neoprene insert and apparently also of the synthetic bones stand out in the dark-field domain. It is, however, evident that the latter modality features a distinctly lower resolution compared to the conventional attenuation image. This is caused by low-frequency artefacts originating from the sliding window phase retrieval approach¹⁰ and is acceptable, since the dark-field signal inherently already contains sub-resolution information.

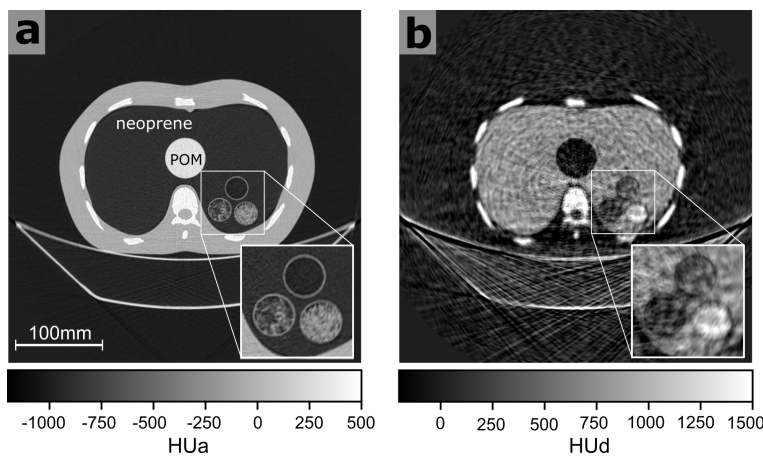


Figure 2. Reconstruction results of an anthropomorphic human chest phantom where a neoprene foam is used to simulate the attenuating and scattering characteristics of lung parenchyma. The field of view (FOV) comprises the whole thorax cross-section along with the patient table. **a**, The conventional reconstruction shows the expected good contrast for bones and a very low signal from the lung area. **b**, In the dark-field reconstruction, homogeneous materials like POM or soft tissue generate no signal, while the scattering properties of the foam material and powdered sugar are clearly retrieved.

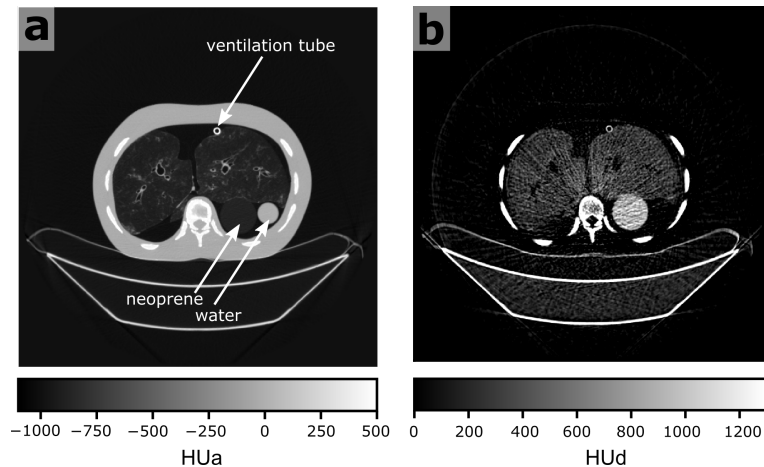


Figure 3. Reconstruction results of a dissected porcine lung placed inside the human chest phantom. **a**, Conventional attenuation reconstruction shows the additional bronchial system while the alveolar structure has comparable attenuation characteristics to the neoprene material. **b**, The scattering properties of the microstructured porcine lung tissue are clearly retrieved in the dark-field, however, the signal is significantly lower compared to the neoprene reference.

5. PORCINE LUNG SAMPLE

Although the used neoprene material features micro-structures in size comparable to pulmonary alveoli, it cannot fully model the anatomical structure of actual lung parenchyma. The phantom material is highly uniform while lung tissue additionally comprises a capillary system and bronchioles of different sizes. We therefore extended the measurements examining a porcine lung. The additional attenuation of human tissue was again modeled by inserting the lung into the thorax phantom along with a water and neoprene reference sample. A dissected porcine lung was ordered from a butcher and the measurements were conducted more than 24 h post-mortem. The lung was inflated externally with 30 mbar in order to partially revert an incipient collapse of lung alveoli.

The resulting attenuation and dark-field images are shown in Fig. 3a and b. From the conventional reconstruction it is evident that the attenuation of lung tissue is similar to the neoprene foam, but also reveals additional bronchi. The scattering properties of the lung tissue are clearly captured in the dark-field domain, however, the signal is significantly lower compared to the neoprene reference material. Previous work with dark-field radiography already showed a significant dependence of the dark-field signal on the applied ventilation pressure.¹⁴ It hence can be justifiably assumed that a higher density of scattering interfaces in the case of a decreased ventilation pressure will favour dark-field signal intensity. Moreover, a further increased signal can also be expected in living subjects since a decomposition processes of lung parenchyma starts immediately after death when the tissue is no longer perfused.

6. NON-CLINICAL APPLICATIONS

Beyond clinical application, dark-field imaging finds general use when examining microscopic defects and fibrous or porous materials in the field of non-destructive testing or for quality control purposes. The key features of the presented dark-field CT prototype system enable new possibilities for applications where the FOV or acquisition time has been a significant limiting factor. Here, we demonstrate a potential for security screening applications with large samples. For this purpose a cloth bag was imaged after filling it with several items along with a sample of fine baby powder. In the attenuation image in Fig. 4a the powder appears to be a microscopically homogeneous object. On the dark-field Hounsfield scale in Fig. 4b it reaches values of up to 13×10^3 HUd which is close to a total extinction of the maximum visibility of the system (see¹⁰). Soft homogeneous materials could be thus efficiently separated from similarly absorbing explosives or drugs that incorporate micro-granular scatterers. Depending on the respective scattering power and the thickness or volume of the material, however, a higher maximum visibility might be required. Moreover, metallic structures which are not uncommon in such applications will be a major challenge for a reasonable performance of a grating interferometer.

7. DOSE CONSIDERATIONS

The presented phantom scans were acquired in axial data acquisition mode using an 80 kVp spectrum and a tube current of 550 mA. The integrated grating interferometer consists out of three optical X-ray gratings which

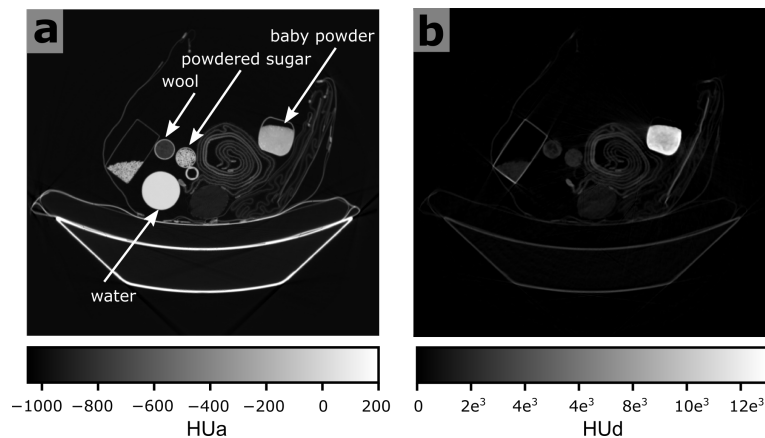


Figure 4. Reconstruction results of a bag filled with different objects (water bottle, wool, powdered sugar, packaging material, rolled towels and cardboard). **a**, In the conventional reconstruction, microgranular powder appears to be homogeneous and cannot be distinguished from bulk material or fluids with similar attenuation. **b**, In the dark-field image, the powder can be clearly differentiated even from other strongly scattering materials like powdered sugar.

absorb a significant part of the generated X-ray flux. With an unmodified CT system, our settings would result in a volume CT dose index ($CTDI_{vol}$) of about 13 mGy. The measured $CTDI_{vol}$ of 7.39 mGy with these settings according to the constancy test protocol¹⁵ with a standard body phantom (32 cm diameter) and a calibrated dosimeter (NOMEX, PTW, Germany) indicates that the combination of the first two gratings can be considered to absorb around 50% of the generated X-ray photons in front of the patient. This value lies well within the clinically applicable range for chest CT of adults at state of the art CT systems.¹⁶ Since one of the absorbing gratings is positioned after the patient directly in front of the detector, a substantial part of the applied patient dose does not actually reach the detector. This is, however, compensated by retrieving sub-resolution information in the additional dark-field modality, which can not be accessed by attenuation contrast only.

8. CONCLUSION

In this work we presented results of recent phantom measurements with the first clinical dark-field CT prototype system. Despite the restrictions posed by the compact interferometer geometry and limitations in current grating fabrication technology, the system performs reasonably well on a sufficient FOV and within a clinically conceivable dose range. We propose a HUD scale for quantitative dark-field imaging and discuss the expected signal strength of lung tissue by means of different phantom materials. Although the presented phantom studies are mainly dedicated to lung imaging, further clinical as well as non-clinical applications are now accessible due to a large FOV in combination with a fast data acquisition procedure.

ACKNOWLEDGMENTS

The authors wish to thank Julia Herzen, Daniela Pfeiffer, Alexander Fingerle, Ernst Rummeny, Pascal Meyer, Jürgen Mohr, Maximilian von Teuffenbach, Amanda Pleier, Tom Kumschier, Michael Heider, Sven Prevrhal, Thomas Reichel, Ami Altman, and Shlomo Gotman for their help, support, and dedication to launch this complex project. This work was carried out with the support of the Karlsruhe Nano Micro Facility (KNMF, www.kit.edu/knmf), a Helmholtz Research Infrastructure at Karlsruhe Institute of Technology (KIT). We acknowledge the support of the TUM Institute for Advanced Study, funded by the German Excellence Initiative, the European Research Council (ERC, H2020, AdG 695045) and Philips GmbH Market DACH.

REFERENCES

- [1] Pfeiffer, F., Bech, M., Bunk, O., Kraft, P., Eikenberry, E. F., Brönnimann, C., Grünzweig, C., and David, C., "Hard-x-ray dark-field imaging using a grating interferometer," *Nat. Mater.* **7**, 134–137 (2008).
- [2] Yashiro, W., Terui, Y., Kawabata, K., and Momose, A., "On the origin of visibility contrast in x-ray Talbot interferometry," *Opt. Express* **18**(16), 16890 (2010).
- [3] Modregger, P., Cremona, T. P., Benarafa, C., Schittny, J. C., Olivo, A., and Endrizzi, M., "Small angle x-ray scattering with edge-illumination," *Sci. Rep.* **6**, 30940 (2016).

- [4] Willer, K., Fingerle, A. A., Noichl, W., De Marco, F., Frank, M., Urban, T., Schick, R., Gustschin, A., Gleich, B., Herzen, J., Koehler, T., Yaroshenko, A., Pralow, T., Zimmermann, G. S., Renger, B., Sauter, A. P., Pfeiffer, D., Makowski, M. R., Rummeny, E. J., Grenier, P. A., and Pfeiffer, F., “X-ray dark-field chest imaging for detection and quantification of emphysema in patients with chronic obstructive pulmonary disease: a diagnostic accuracy study,” *The Lancet Digital Health* **3**(11), e733–e744 (2021).
- [5] Yaroshenko, A., Hellbach, K., Yildirim, A. Ö., Conlon, T. M., Fernandez, I. E., Bech, M., Velroyen, A., Meinel, F. G., Auweter, S., Reiser, M., Eickelberg, O., and Pfeiffer, F., “Improved In vivo Assessment of Pulmonary Fibrosis in Mice using X-Ray Dark-Field Radiography,” *Sci. Rep.* **5**, 17492 (2015).
- [6] Scherer, K., Yaroshenko, A., Bölükbas, D. A., Gromann, L. B., Hellbach, K., Meinel, F. G., Braunagel, M., Von Berg, J., Eickelberg, O., Reiser, M. F., Pfeiffer, F., Meiners, S., and Herzen, J., “X-ray Dark-field Radiography - In-Vivo Diagnosis of Lung Cancer in Mice,” *Sci. Rep.* **7**(1), 402 (2017).
- [7] Momose, A., “X-ray phase imaging reaching clinical uses,” *Phys. Med.* **79**, 93–102 (2020).
- [8] Velroyen, A., Yaroshenko, A., Hahn, D., Fehring, A., Tapfer, A., Müller, M., Noël, P. B., Pauwels, B., Sasov, A., Yildirim, A., Eickelberg, O., Hellbach, K., Auweter, S. D., Meinel, F. G., Reiser, M. F., Bech, M., and Pfeiffer, F., “Grating-based X-ray Dark-field Computed Tomography of Living Mice,” *EBioMedicine* **2**(10), 1500–1506 (2015).
- [9] Wu, Z., Wei, W. B., Gao, K., Liu, G., Liu, G. F., Sun, H. X., Jiang, J., Wang, Q. P., Lu, Y. L., and Tian, Y. C., “Prototype system of non-interferometric phase-contrast computed tomography utilizing medical imaging components,” *J. Appl. Phys.* **129**(7), 074901 (2021).
- [10] Viermetz, M., Gustschin, N., Schmid, C., Haeusele, J., von Teuffenbach, M., Meyer, P., Bergner, F., Lasser, T., Proksa, R., Koehler, T., and Pfeiffer, F., “Dark-field computed tomography reaches the human scale,” *PNAS* **119**(8), e2118799119 (2022).
- [11] Bech, M., Bunk, O., Donath, T., Feidenhans'l, R., David, C., and Pfeiffer, F., “Quantitative x-ray dark-field computed tomography,” *Phys. Med. Biol.* **55**, 5529–5539 (2010).
- [12] “Multipurpose Chest Phantom N1 ”LUNGMAN”.” https://www.kyotokagaku.com/en/products_data/ph-1_01/ (2020). (accessed 03 January 2021).
- [13] Taphorn, K., De Marco, F., Andrejewski, J., Sellerer, T., Pfeiffer, F., and Herzen, J., “Grating-based spectral X-ray dark-field imaging for correlation with structural size measures,” *Sci. Rep.* **10**, 13195 (2020).
- [14] Marco, F. D., Willer, K., Gromann, L. B., Andrejewski, J., Hellbach, K., Bähr, A., Dmochewitz, M., Koehler, T., Maack, H.-I., Pfeiffer, F., and Herzen, J., “Contrast-to-noise ratios and thickness-normalized, ventilation-dependent signal levels in dark-field and conventional in vivo thorax radiographs of two pigs,” *PLOS ONE* **14**, e0217858 (2019).
- [15] IEC 61223-2-6:2006, “Evaluation and routine testing in medical imaging departments - Constancy tests,” (2006).
- [16] American Association of Physicists in Medicine, “Adult Routine Chest CT Protocols.” <https://www.aapm.org/pubs/CTProtocols/> (May 2016). (accessed 10 December 2021).